

Modal substructuring of geometrically nonlinear finite element models with interface reduction

Robert J. Kuether^{*},

Sandia National Laboratories¹, Albuquerque, New Mexico, 87185

Matthew S. Allen[†]

Department of Engineering Physics, University of Wisconsin-Madison, Madison, Wisconsin, 53706
and

Joseph J. Hollkamp[‡]

U.S. Air Force Research Laboratory, Wright-Patterson Air Force Base, Ohio, 45433

Substructuring methods have been widely used in structural dynamics to divide large, complicated finite element models into smaller substructures. For linear systems, many methods have been developed to reduce the subcomponents down to a low order set of equations using a special set of component modes, and these are then assembled to approximate the dynamics of a large scale model. In this paper, a substructuring approach is developed for coupling geometrically nonlinear structures, where each subcomponent is drastically reduced to a low order set of nonlinear equations using a truncated set of fixed-interface and characteristic constraint modes. The method used to extract the coefficients of the nonlinear reduced order model (NLROM) is non-intrusive in that it does not require any modification to the commercial FEA code, but computes the NLROM from the results of several nonlinear static analyses. The NLROMs are then assembled to approximate the nonlinear differential equations of the global assembly. The method is demonstrated on the coupling of two geometrically nonlinear plates with simple supports at all edges. The plates are joined at a continuous interface through the rotational degrees-of-freedom (DOF), and the nonlinear normal modes (NNMs) of the assembled equations are computed to validate the models. The proposed substructuring approach reduces a 12,861 DOF nonlinear finite element model down to only 23 DOF, while still accurately reproducing the first three NNMs of the full order model.

Nomenclature

B_r, A_r	=	quadratic and cubic nonlinear stiffness, respectively
\mathbf{F}_d	=	vector of applied static forces using Implicit Condensation and Expansion
$\mathbf{f}_{NL}(\mathbf{x})$	=	vector of nonlinear restoring forces
$\mathbf{f}(t)$	=	vector of external forces
\hat{f}_r	=	scaling for the r^{th} mode using Implicit Condensation and Expansion

^{*} Senior Member of Technical Staff, P.O. Box 5800, rjkueth@sandia.gov.

[†] Associate Professor, 535 Engineering Research Building, 1500 Engineering Drive, Madison, WI 53706-1609, msallen@engr.wisc.edu, AIAA Lifetime Member.

[‡] Senior Aerospace Engineer, Structural Sciences Center, AFRL/RQHF, 2790 D Street, Building 65, Wright-Patterson Air Force Base, OH 45433, Joseph.Hollkamp@us.af.mil.

¹Sandia National Laboratories is a multi-program laboratory managed and operated by Sandia Corporation, a wholly owned subsidiary of Lockheed Martin Corporation, for the U.S. Department of Energy's National Nuclear Security Administration under contract DE-AC04-94AL85000.

\mathbf{I}	= identity matrix
\mathbf{K}	= linear stiffness matrix
$\hat{\mathbf{K}}_{CC}$	= CC reduced stiffness matrix
\mathbf{L}	= connectivity matrix
\mathbf{M}	= linear mass matrix
$\hat{\mathbf{M}}_{CC}$	= CC reduced mass matrix
$\mathbf{N}_1(\mathbf{q})$	= Quadratic nonlinear modal stiffness matrix
$\mathbf{N}_2(\mathbf{q})$	= Cubic nonlinear modal stiffness matrix
\mathbf{p}, \mathbf{q}	= vector of modal coordinates
\mathbf{p}_u	= vector of unconstrained modal coordinates
\mathbf{q}_c	= vector of characteristic constraint modal coordinates
\mathbf{q}_k	= vector of fixed-interface modal coordinates
$\mathbf{r}(t)$	= vector of reaction forces
\mathbf{T}_{CB}	= Craig-Bampton transformation matrix
\mathbf{T}_{CC}	= fixed-interface with characteristic constraint modes transformation matrix
$\mathbf{x}, \ddot{\mathbf{x}}$	= vector of displacements and accelerations, respectively
Φ	= fixed-interface mode shape matrix
ϕ	= mass normalized fixed-interface mode shape vector
Λ	= diagonal matrix of fixed-interface modal frequencies
$\theta(\mathbf{q})$	= nonlinear modal restoring force
ω	= linear natural frequency
ψ	= boundary mode shape vector
Ψ	= constraint mode shape matrix
$\hat{\Psi}$	= characteristic constraint mode shape matrix
$()^T$	= transpose operator

$()^\dagger$ = pseudo-inverse operator

Keywords: substructuring, component mode synthesis, geometric nonlinearity, interface reduction, nonlinear normal modes.

I. Introduction

Structures with geometric nonlinearities [1, 2], or large deformations, can be encountered in thin-walled members while the materials remain linear elastic. Model reduction on these types of systems have been motivated in the last decade or so by NASA [3-7] and the United States Air Force [8-11] to design and model structural components of reusable hypersonic aircraft using finite element analysis (FEA). Extreme thermal, pressure and acoustic loads during flight can cause the external skin panels to vibrate with large response amplitudes requiring FEA analysis with geometric nonlinearity to model structures with detailed geometric features (e.g. stiffeners or curved surfaces). This work addresses some of the challenges associated with model reduction of such geometrically nonlinear FEA models by developing a modal substructuring, or component mode synthesis (CMS), approach. This is accomplished by first dividing the structure of interest into two or more subcomponent FEA models, reducing each of these sub-models to a low order set of nonlinear modal equations, and coupling them to obtain a model of the assembly. In the present work, we propose to reduce the nonlinear subcomponent models using the Implicit Condensation and Expansion (ICE) approach in [8, 9] with the fixed-interface and characteristic constraint modes that were originally derived in [12], which reduces the number of static constraint modes at the interface. This reduction drastically reduces the upfront CPU cost of creating reduced order models (ROMs) with ICE along with the order of the assembled model.

The existing CMS approaches in the literature differ by the types of component modes, or Ritz vectors, used to reduce the FEA model. The first substructuring method developed for linear systems was presented by Hurty in [13] using fixed-interface vibration modes, which Craig and Bampton later simplified in [14]; other methods based on free-interface vibration modes were developed later in [15-18]. The Craig-Bampton (CB) substructuring approach [14] reduces each subcomponent model with fixed-interface modes and static constraint modes to account for deformation at the interface. For FEA models with many connecting degrees-of-freedom (DOF), these reduced order models may still be prohibitively large since one constraint mode is needed for each interface DOF. Furthermore, the CB basis may become ineffective with a high density of closely spaced nodes on the interface [19]. Castanier et al. developed system-level characteristic constraint (S-CC) modes in [12] where they perform a secondary modal

analysis on the interface DOF of the assembled CB models in order to reduce the number of static constraint modes, or interface DOF. Later, Hong et al. [20] developed local characteristic constraint (L-CC) modes for local interface reduction by solving a secondary modal analysis of a CB ROM at the subcomponent level, allowing for the CC modes to be calculated without knowledge of the adjacent structure(s). Others works regarding interface reduction can be found in [21-23].

A variety of indirect methods have been developed to generate ROMs of geometrically nonlinear finite element models built directly within commercial FEA packages, as reviewed in [10, 24]. These methods project a set of component modes onto the nonlinear FEA equations of motion to obtain a set of low order, nonlinear modal equations. In commercially available FEA software, the linear mass and stiffness matrices can be readily exported, however the nonlinear stiffness terms due to geometric nonlinearity cannot. Therefore, an indirect approach is needed to identify the nonlinear portion of the modal model (i.e. a quadratic and cubic polynomial function of modal coordinates) using a series of static load cases with either applied forces [8, 9, 25] or enforced displacements [3, 26]. The resulting model offers significant computational savings for response prediction compared to the direct integration of the full order model. Several existing works to date reduce the monolithic FEA model with its linear vibrations modes [3, 7, 10, 25-28], although the enforced displacements procedure sometimes augments bending vibrations modes with a set of dual [27] or companion [29] modes to capture in-plane kinematics. More recently, other modes such as fixed-interface modes with static constraint modes have been used to create reduced subcomponent FEA models for the purpose of substructuring (e.g. see [30-32]).

Most developments of the indirect model reduction approach have sought to generate a ROM of a structure using its monolithic FEA model. While this approach has been very effective for many studies, it becomes exceedingly expensive if the system requires many modal DOF to capture the kinematics, in turn requiring a prohibitively large number of static load cases to fit the nonlinear stiffness coefficients. For example, to fit the coefficients for a 20-mode model using ICE, one must apply 9,920 permutations of static loads, whereas a 50-mode and a 100-mode model would require 161,800 and 1,313,600, respectively [8]. This cost has been addressed to some extent using the enforced displacement procedure in [26], which uses the tangent stiffness matrix to more efficiently compute the polynomial coefficients, requiring the number of static loads on the order of N^2 compared to N^3 with the ICE method (where N is the number of modes in the basis). They demonstrated the procedure by reducing a 96,000 DOF model of a 9-bay panel to an 85-mode model, but even then it was challenging to determine which modes to include and

what displacements to apply to determine the nonlinear stiffness. A modal substructuring approach divides a large, complicated model into smaller subcomponents, each of which are far simpler and easier to create a validated model. The subcomponent models can then be assembled to generate a global ROM of the assembly that takes into account the effects of geometric nonlinearity. Another advantage to the substructuring approach is that during the design stage the subcomponents are typically redesigned by different teams and independently of the global structure, and so it is more convenient to modify and recompute the models for smaller, simpler subcomponents rather than a larger, global model.

A modal substructuring approach for geometrically nonlinear FEA models is proposed here by generating subcomponent ROMs using the ICE procedure reduced with fixed-interface and characteristic constraint (CC) modes that are then assembled using a primal approach, just as done with linear systems [33, 34]. The authors first explored this approach by assembling subcomponent ROMs reduced with free-interface modes [35], but it was found that far too many modes were required to obtain acceptable accuracy. Later the authors explored the use of fixed-interface and constraint modes (e.g. Craig-Bampton modes) on an assembly of two geometrically nonlinear beams [30, 32], where the connecting interface had only one DOF. This approach performed very well for a model with a simple interface, however for a continuous interface with more than a few DOF, the number of constraint modes would prohibit the use of the ICE approach, hence motivating the use of characteristic constraint modes. Perez was the first to suggest the use of this basis on a complicated multi-bay panel with the enforced displacements procedure in [31]. He found that a linear substructuring approach could reduce the linear model from 96,000 DOF to 232 DOF using fixed-interface and constraint modes reduced using proper orthogonal decomposition. The nonlinear modal substructuring was not actually pursued in his work as the reduction of the monolithic structure only required 89 DOF using linear bending modes and dual modes.

The paper is outlined as follows. Section II presents the theory behind the synthesis of nonlinear reduced order models created with fixed-interface and characteristic constraint modes (abbreviated as CC-NLROMs). This section also discusses two methodologies to compute the characteristic constraint modes and how to use these in a substructuring framework (i.e. how to assemble the reduced models created with each basis). The modal substructuring approach is then demonstrated in Section III on an example problem where two geometrically nonlinear flat plates with simple supports at all the edges are coupled at a continuous interface through the rotational degrees-of-freedom. The nonlinear normal modes (NNMs) of the assembly are used to evaluate the accuracy of the

assembled CC-NLROMs by comparing them to NNMs computed directly from the full order model of the plate assembly. This work defines the undamped NNM [36] as a *not necessarily synchronous periodic response of the undamped nonlinear equations of motion*, which has been found to provide a useful metric to evaluate the modal convergence of a nonlinear ROM [28, 30, 37, 38]. The conclusions are presented in Section IV.

II. Theory

A modal substructuring procedure for structural dynamic analysis first divides the global structure of interest into smaller substructures, whose equations are reduced at the subcomponent level before being assembled to provide a reduced order model. Therefore, we start with the spatially discretized, geometrically nonlinear finite element model of a subcomponent, giving the undamped, N -DOF equations of motion in the form,

$$\mathbf{M}\ddot{\mathbf{x}} + \mathbf{K}\mathbf{x} + \mathbf{f}_{NL}(\mathbf{x}) = \mathbf{f}(t) \quad (1)$$

Here, \mathbf{M} and \mathbf{K} are the $N \times N$ linear mass and stiffness matrices, respectively, and $\mathbf{f}_{NL}(\mathbf{x})$ is the $N \times 1$ nonlinear restoring force vector that accounts for the internal forces due to geometric nonlinearity. The $N \times 1$ vectors \mathbf{x} , $\ddot{\mathbf{x}}$, and $\mathbf{f}(t)$ are the displacement, acceleration and external forces, respectively. The nonlinear modal substructuring procedure is outlined in the following three steps, each of which is covered in the subsections below.

- A. Select the subcomponent modal basis to reduce each subcomponent FEA model in Eq. (1).
- B. Generate the reduced modal equations with the basis defined in step A.
- C. Couple the nonlinear subcomponent models to obtain a reduced order model of the assembly.

A. Fixed-interface Modes and Characteristic Constraint Modes

In order to reduce each subcomponent FEA model, first a set of subcomponent modes, or Ritz vectors, are needed to capture the kinematics of each substructure. This work uses the fixed-interface modes and characteristic constraint modes developed in [12] and [20]; the theory is reviewed here. Note that any appropriate modal basis could be used, such as those developed for the other existing linear substructuring procedures reviewed earlier, however these bases are chosen because of the reduction on the interface DOF. Starting with the *linear* form of the equations of motion in Eq. (1) (i.e. when $\mathbf{f}_{NL}(\mathbf{x}) = \mathbf{0}$), each DOF in \mathbf{x} is partitioned into either boundary DOF, \mathbf{x}_b , or interior DOF, \mathbf{x}_i . The boundary DOF are either shared by an adjacent structure, sometimes referred to as

interface DOF, or may have an external point load $\mathbf{f}(t)$ applied to that location. The interior DOF are all the remaining coordinates of the system. The partitioned equations of motion of the full order, linear model become

$$\begin{bmatrix} \mathbf{M}_{ii} & \mathbf{M}_{ib} \\ \mathbf{M}_{bi} & \mathbf{M}_{bb} \end{bmatrix} \begin{Bmatrix} \ddot{\mathbf{x}}_i \\ \ddot{\mathbf{x}}_b \end{Bmatrix} + \begin{bmatrix} \mathbf{K}_{ii} & \mathbf{K}_{ib} \\ \mathbf{K}_{bi} & \mathbf{K}_{bb} \end{bmatrix} \begin{Bmatrix} \mathbf{x}_i \\ \mathbf{x}_b \end{Bmatrix} = \begin{Bmatrix} \mathbf{0} \\ \mathbf{f}(t) \end{Bmatrix} \quad (2)$$

The fixed-interface modes are computed by restraining all the boundary coordinates, \mathbf{x}_b , and solving the eigenvalue problem $(\mathbf{K}_{ii} - \omega_r^2 \mathbf{M}_{ii}) \boldsymbol{\phi}_r = \mathbf{0}$ from the linear system matrices partitioned to only the interior DOF, \mathbf{x}_i , in Eq. (2). These fixed-interface modes are then mass normalized with respect to \mathbf{M}_{ii} . These shapes are augmented with a set of static shapes, known as constraint modes, which account for deformations at the boundary, or interface, DOF. One constraint mode is computed for every boundary coordinate in \mathbf{x}_b by computing the static deflection to a unit displacement at each boundary DOF while holding all the other boundary coordinates fixed. These shapes are computed as,

$$\boldsymbol{\Psi} = \begin{bmatrix} \boldsymbol{\Psi}_{ib} \\ \mathbf{I}_{bb} \end{bmatrix} = \begin{bmatrix} -\mathbf{K}_{ii}^{-1} \mathbf{K}_{ib} \\ \mathbf{I}_{bb} \end{bmatrix} \quad (3)$$

The modal transformation matrix with fixed-interface modes and constraint modes then becomes,

$$\begin{Bmatrix} \mathbf{x}_i \\ \mathbf{x}_b \end{Bmatrix} = \begin{bmatrix} \boldsymbol{\Phi}_{ik} & \boldsymbol{\Psi}_{ib} \\ \mathbf{0} & \mathbf{I} \end{bmatrix} \begin{Bmatrix} \mathbf{q}_k \\ \mathbf{x}_b \end{Bmatrix} = \mathbf{T}_{CB} \mathbf{q} \quad (4)$$

where $\boldsymbol{\Phi}_{ik}$ is the $N_i \times N_k$ matrix of mass normalized fixed-interface modes, \mathbf{I} is the identity matrix, and $\boldsymbol{\Psi}_{ib}$ is the $N_i \times N_b$ matrix of constraint modes. The number of fixed-interface modes needed in the basis depends on the desired level of accuracy of the assembled ROMs. The total number of modal coordinates in the vector \mathbf{q} is the number of retained fixed-interface modes, N_k , plus the number of constraint modes N_b , denoted as $m = N_k + N_b$. The resulting $N \times m$ matrix \mathbf{T}_{CB} is referred as the Craig-Bampton transformation matrix in [14, 33].

A CB reduced order model of the subcomponent is created by substituting Eq. (4) into Eq. (2) and pre-multiplying by the transpose, $()^T$, of the CB transformation matrix, \mathbf{T}_{CB}^T , to give the form,

$$\begin{bmatrix} \mathbf{I}_{kk} & \hat{\mathbf{M}}_{kb} \\ \hat{\mathbf{M}}_{bk} & \hat{\mathbf{M}}_{bb} \end{bmatrix} \begin{Bmatrix} \ddot{\mathbf{q}}_k \\ \ddot{\mathbf{x}}_b \end{Bmatrix} + \begin{bmatrix} \boldsymbol{\Lambda}_{kk} & \mathbf{0}_{kb} \\ \mathbf{0}_{bk} & \hat{\mathbf{K}}_{bb} \end{bmatrix} \begin{Bmatrix} \mathbf{q}_k \\ \mathbf{x}_b \end{Bmatrix} = \begin{Bmatrix} \mathbf{0} \\ \mathbf{f}(t) + \mathbf{r}(t) \end{Bmatrix} \quad (5)$$

The vector $\mathbf{r}(t)$ is added here and accounts for the unknown equal and opposite reaction force that will be applied by an adjacent structure, and $\boldsymbol{\Lambda}_{kk}$ is a diagonal matrix of squared natural frequencies of the fixed-interface modes. For FEA models with very detailed meshes at the interface, there may be many thousands of DOF at the boundary requiring many constraint modes in $\boldsymbol{\Psi}$. A reduction of these boundary coordinates, \mathbf{x}_b , can be achieved using two (slightly) different approaches involving a secondary modal analysis.

1. System-level Characteristic Constraint (S-CC) Modes [12]

This approach is initiated by first assembling all the linear CB models from Eq. (5) using the primal formulation [14, 33]. Without loss of generality, coupling two linear subcomponents denoted with superscripts (A) and (B) produces the equations of motion of the assembly

$$\begin{bmatrix} \mathbf{I}_{k_A k_A}^{(A)} & \mathbf{0} & \hat{\mathbf{M}}_{k_A b}^{(A)} \\ \mathbf{0} & \mathbf{I}_{k_B k_B}^{(B)} & \hat{\mathbf{M}}_{k_B b}^{(B)} \\ \hat{\mathbf{M}}_{b k_A}^{(A)} & \hat{\mathbf{M}}_{b k_B}^{(B)} & \hat{\mathbf{M}}_{bb}^{(A)} + \hat{\mathbf{M}}_{bb}^{(B)} \end{bmatrix} \begin{Bmatrix} \ddot{\mathbf{q}}_{k_A}^{(A)} \\ \ddot{\mathbf{q}}_{k_B}^{(B)} \\ \ddot{\mathbf{x}}_b \end{Bmatrix} + \begin{bmatrix} \boldsymbol{\Lambda}_{k_A k_A}^{(A)} & \mathbf{0} & \mathbf{0} \\ \mathbf{0} & \boldsymbol{\Lambda}_{k_B k_B}^{(B)} & \mathbf{0} \\ \mathbf{0} & \mathbf{0} & \hat{\mathbf{K}}_{bb}^{(A)} + \hat{\mathbf{K}}_{bb}^{(B)} \end{bmatrix} \begin{Bmatrix} \mathbf{q}_{k_A}^{(A)} \\ \mathbf{q}_{k_B}^{(B)} \\ \mathbf{x}_b \end{Bmatrix} = \begin{Bmatrix} \mathbf{0} \\ \mathbf{0} \\ \mathbf{f}(t) \end{Bmatrix} \quad (6)$$

A second modal analysis is performed on the *assembled* linear mass and stiffness matrices corresponding to the boundary DOF, \mathbf{x}_b , in Eq. (6) by solving the eigenvalue problem

$$\left((\hat{\mathbf{K}}_{bb}^{(A)} + \hat{\mathbf{K}}_{bb}^{(B)}) - \omega_r^2 (\hat{\mathbf{M}}_{bb}^{(A)} + \hat{\mathbf{M}}_{bb}^{(B)}) \right) \boldsymbol{\Psi}_{S-CC,r} = \mathbf{0} \quad (7)$$

These boundary eigenvectors, $\boldsymbol{\Psi}_{S-CC,r}$, are truncated and used to assemble the $N_b \times N_c$ matrix $\boldsymbol{\Psi}_{S-CC}$. The work in [12] uses this reduction to further reduce the assembled ROMs in Eq. (6), however the present study uses this to reduce the constraint modes in the CB transformation matrix in Eq. (4) as,

$$\mathbf{x} = \begin{Bmatrix} \mathbf{x}_i \\ \mathbf{x}_b \end{Bmatrix} = \begin{bmatrix} \boldsymbol{\Phi}_{ik} & \boldsymbol{\Psi}_{ib} \\ \mathbf{0} & \mathbf{I} \end{bmatrix} \begin{bmatrix} \mathbf{I} & \mathbf{0} \\ \mathbf{0} & \boldsymbol{\Psi}_{S-CC} \end{bmatrix} \begin{Bmatrix} \mathbf{q}_k \\ \mathbf{q}_c \end{Bmatrix} = \begin{bmatrix} \boldsymbol{\Phi}_{ik} & \hat{\boldsymbol{\Psi}}_{ic} \\ \mathbf{0} & \hat{\boldsymbol{\Psi}}_{bc} \end{bmatrix} \begin{Bmatrix} \mathbf{q}_k \\ \mathbf{q}_c \end{Bmatrix} = \mathbf{T}_{S-CC} \mathbf{p} \quad (8)$$

$\hat{\Psi} = \begin{bmatrix} \hat{\Psi}_{ic}^T & \hat{\Psi}_{bc}^T \end{bmatrix}^T$ is now the $N \times N_c$ matrix of system-level characteristic constraint modes that capture the "characteristic" motion of the interface for a single subcomponent. The total number of generalized coordinates in the vector \mathbf{p} becomes $l = N_k + N_c$, and the $N \times l$ matrix \mathbf{T}_{S-CC} contains the fixed-interface modes and the system-level characteristic constraint modes. The generalized coordinates in the $l \times 1$ vector \mathbf{p} have significantly fewer DOF than total number of N physical DOF in Eq. (1), and the m CB modal coordinates in Eq. (4). Note that with this approach, the compatibility of all the connecting DOF is achieved with the primal assembly of the CB models in Eq. (6), which ensures that the constraints along the interface are exactly enforced. The implications of this during the synthesis of the ROMs will be discussed further in subsection C.

2. Local Characteristic Constraint (L-CC) Modes [20]

The preceding developments presume that the linear CB models are small enough to synthesize in order to compute the characteristic constraint modes from the linear assembly. In some cases, it might be preferable to reduce the interface without having to first assemble the subcomponents. One way to do this is to reduce the interface DOF of each substructure separately. Specifically, a secondary modal analysis is performed on the single subcomponent in Eq. (5) as,

$$\left(\hat{\mathbf{K}}_{bb} - \omega_r^2 \hat{\mathbf{M}}_{bb} \right) \boldsymbol{\Psi}_{L-CC,r} = \mathbf{0} \quad (9)$$

The boundary eigenvectors, $\boldsymbol{\Psi}_{L-CC,r}$, are also truncated and used in the $N_b \times N_c$ matrix $\boldsymbol{\Psi}_{L-CC}$ (note that with this approach, N_c can vary for each subcomponent). These shapes are then used to reduce the constraint modes in the CB transformation matrix in Eq. (4) as,

$$\mathbf{x} = \begin{Bmatrix} \mathbf{x}_i \\ \mathbf{x}_b \end{Bmatrix} = \begin{bmatrix} \boldsymbol{\Phi}_{ik} & \boldsymbol{\Psi}_{ib} \\ \mathbf{0} & \mathbf{I} \end{bmatrix} \begin{bmatrix} \mathbf{I} & \mathbf{0} \\ \mathbf{0} & \boldsymbol{\Psi}_{L-CC} \end{bmatrix} \begin{Bmatrix} \mathbf{q}_k \\ \mathbf{q}_c \end{Bmatrix} = \begin{bmatrix} \boldsymbol{\Phi}_{ik} & \hat{\boldsymbol{\Psi}}_{ic} \\ \mathbf{0} & \hat{\boldsymbol{\Psi}}_{bc} \end{bmatrix} \begin{Bmatrix} \mathbf{q}_k \\ \mathbf{q}_c \end{Bmatrix} = \mathbf{T}_{L-CC} \mathbf{p} \quad (10)$$

Again, the total number of generalized coordinates in the vector \mathbf{p} becomes $l = N_k + N_c$, where now the $N \times l$ matrix \mathbf{T}_{L-CC} contains the fixed-interface modes and the local characteristic constraint modes. This interface reduction does not account for the mass and stiffness of the adjacent structures, and does not guarantee compatibility along the interface DOF. However, this allows for a reduction to be performed without knowledge of the adjacent

subcomponent models, which may be desirable for re-analysis of assemblies requiring various configurations. The next subsection uses the modal bases derived in either Eq. (8) or Eq. (10) to reduce the *geometrically nonlinear* subcomponent model.

B. Subcomponent Reduced Order Models with Geometric Nonlinearity

In order to reduce the geometrically nonlinear, full order model in Eq. (1), again the displacements, \mathbf{x} , must be sorted into the boundary and interior DOF as,

$$\begin{bmatrix} \mathbf{M}_{ii} & \mathbf{M}_{ib} \\ \mathbf{M}_{bi} & \mathbf{M}_{bb} \end{bmatrix} \begin{Bmatrix} \ddot{\mathbf{x}}_i \\ \ddot{\mathbf{x}}_b \end{Bmatrix} + \begin{bmatrix} \mathbf{K}_{ii} & \mathbf{K}_{ib} \\ \mathbf{K}_{bi} & \mathbf{K}_{bb} \end{bmatrix} \begin{Bmatrix} \mathbf{x}_i \\ \mathbf{x}_b \end{Bmatrix} + \begin{Bmatrix} \mathbf{f}_{NL,i}(\mathbf{x}) \\ \mathbf{f}_{NL,b}(\mathbf{x}) \end{Bmatrix} = \begin{Bmatrix} \mathbf{0} \\ \mathbf{f}(t) \end{Bmatrix} \quad (11)$$

Here, either transformation matrix Eq. (8) or Eq. (10) can be used to reduce these equations, and will be referred generally as \mathbf{T}_{CC} since the procedure is the same for either basis. The coordinate transformation is substituted into Eq. (11) and the resulting equations are premultiplied by \mathbf{T}_{CC}^T to create the CC-NLROM equations of motion,

$$\hat{\mathbf{M}}_{CC} \ddot{\mathbf{p}} + \hat{\mathbf{K}}_{CC} \mathbf{p} + \mathbf{T}_{CC}^T \begin{Bmatrix} \mathbf{f}_{NL,i}(\mathbf{T}_{CC} \mathbf{p}) \\ \mathbf{f}_{NL,b}(\mathbf{T}_{CC} \mathbf{p}) \end{Bmatrix} = \mathbf{T}_{CC}^T \begin{Bmatrix} \mathbf{0} \\ \mathbf{f}(t) + \mathbf{r}(t) \end{Bmatrix} \quad (12)$$

It is assumed that the subcomponent FEA models are created in a commercial software package, so the unknown nonlinear modal restoring force can be defined generally as

$$\mathbf{T}_{CC}^T \begin{Bmatrix} \mathbf{f}_{NL,i}(\mathbf{T}_{CC} \mathbf{p}) \\ \mathbf{f}_{NL,b}(\mathbf{T}_{CC} \mathbf{p}) \end{Bmatrix} = \boldsymbol{\theta}(p_1, p_2, \dots, p_l) \quad (13)$$

The nonlinear function $\boldsymbol{\theta}(p_1, p_2, \dots, p_l)$ depends on each of the modal coordinates, \mathbf{p} , in the reduction basis. Many common large displacement strain models [1, 2] have shown that $\mathbf{f}_{NL}(\mathbf{x})$ is expressible as a quadratic and cubic polynomial function, therefore the same functional form will hold for the modal form of the equations, as done in [10, 24]. Therefore, the r^{th} row of the nonlinear modal restoring force is given as,

$$\theta_r(p_1, p_2, \dots, p_l) = \sum_{i=1}^l \sum_{j=i}^l B_r(i, j) p_i p_j + \sum_{i=1}^l \sum_{j=i}^l \sum_{k=j}^l A_r(i, j, k) p_i p_j p_k \quad (14)$$

The nonlinear stiffness coefficients A_r and B_r are not explicitly available when the FEA models are built directly in a commercial software package, so an indirect approach [10, 24] is used to determine these values.

This work uses the Implicit Condensation and Expansion method in [9] to estimate the unknown coefficients by applying a series of static forces to the full, nonlinear FEA substructure model in Eq. (1). The FEA software performs the static analyses to determine the resulting deformations to a permutation of static forces that are the sums and differences of either one, two or three of the component modes in \mathbf{T}_{CC} . For example, the d^{th} static force combination of the r^{th} , s^{th} , and v^{th} mode shapes can be arbitrarily defined as

$$\mathbf{F}_d = \begin{bmatrix} \mathbf{K}_{ii} & \mathbf{K}_{ib} \\ \mathbf{K}_{bi} & \mathbf{K}_{bb} \end{bmatrix} \left(\mathbf{T}_{CC,r} \hat{f}_r + \mathbf{T}_{CC,s} \hat{f}_s + \mathbf{T}_{CC,v} \hat{f}_v \right) \quad (15)$$

The load scaling factors \hat{f}_r , \hat{f}_s , and \hat{f}_v correspond to the force amplitude applied for the mode in the r^{th} , s^{th} , and v^{th} column of the matrix \mathbf{T}_{CC} , and \mathbf{F}_d is an $N \times 1$ static force vector for the d^{th} load case. A set of these force permutations and the computed responses are used with the unconstrained least squares approach to fit the unknown coefficients A_r and B_r . More details on this fitting procedure can be found in [8], and more specific details on the load scaling and force permutations can be found in [8, 30].

There is an upfront CPU cost incurred by the ICE procedure as a result of the static analyses required to fit the modal equations. The number of load cases to fit Eq. (14) scales as

$$\# \text{ load cases} = 2l + \frac{2!}{(l-2)!} + \frac{4!}{3(l-3)!} \quad (16)$$

where again l is the total number of modes used in the basis. One advantage of the ICE procedure is that only bending type fixed-interface modes need to be included in the transformation matrix \mathbf{T}_{CC} since the effects of membrane-bending coupling are implicitly captured when fitting the coefficients, hence reducing the number of required static load cases. Also, the system-level or local characteristic constraint modes offer a more efficient basis by drastically reducing the number of constraint modes, thus improving the upfront computational cost to fit these models. Since the basis does not have any membrane or axial type motions, the expansion process discussed in [9,

30] can be used as a post processing step to accurately capture the in-plane deformations caused by the geometric nonlinearity, ultimately allowing these models to accurately predict strains and stresses.

C. Primal Assembly of Nonlinear Subcomponent Models

The subcomponent models, termed CC-NLROMs, are coupled to any adjacent nonlinear (or possibly linear) substructure(s) using a primal formulation to satisfy the compatibility and equilibrium conditions at the interface. Without loss of generality, consider the assembly of two CC-NLROMs, denoted as (A) and (B), whose equations of motion are given by Eqs. (12)-(14). To join these two structures, only the compatibility condition at the boundary DOF need be satisfied (i.e. $\mathbf{x}_b^{(A)} = \mathbf{x}_b^{(B)}$). Assembling the equations using standard finite element techniques causes the unknown reaction forces at the boundary to cancel, and the equations of motion for the assembled system becomes,

$$\begin{aligned} \mathbf{L}^T \begin{bmatrix} \hat{\mathbf{M}}_{CC}^{(A)} & \mathbf{0} \\ \mathbf{0} & \hat{\mathbf{M}}_{CC}^{(B)} \end{bmatrix} \mathbf{L} \ddot{\mathbf{p}}_u + \mathbf{L}^T \begin{bmatrix} \hat{\mathbf{K}}_{CC}^{(A)} & \mathbf{0} \\ \mathbf{0} & \hat{\mathbf{K}}_{CC}^{(B)} \end{bmatrix} \mathbf{L} \mathbf{p}_u + \frac{1}{2} \mathbf{L}^T \begin{bmatrix} \mathbf{N}_1^{(A)}(\mathbf{p}^{(A)}) & \mathbf{0} \\ \mathbf{0} & \mathbf{N}_1^{(B)}(\mathbf{p}^{(B)}) \end{bmatrix} \mathbf{L} \mathbf{p}_u \\ + \frac{1}{3} \mathbf{L}^T \begin{bmatrix} \mathbf{N}_2^{(A)}(\mathbf{p}^{(A)}) & \mathbf{0} \\ \mathbf{0} & \mathbf{N}_2^{(B)}(\mathbf{p}^{(B)}) \end{bmatrix} \mathbf{L} \mathbf{p}_u = \mathbf{L}^T \begin{Bmatrix} \mathbf{T}_{CC}^{(A)T} \begin{Bmatrix} \mathbf{0} \\ \mathbf{f}(t)^{(A)} \end{Bmatrix} \\ \mathbf{T}_{CC}^{(B)T} \begin{Bmatrix} \mathbf{0} \\ \mathbf{f}(t)^{(B)} \end{Bmatrix} \end{Bmatrix} \end{aligned} \quad (17)$$

The subcomponent matrices $\mathbf{N}_1(\mathbf{p})$ and $\mathbf{N}_2(\mathbf{p})$ are the quadratic and cubic nonlinear stiffness matrices, respectively, for each subcomponent, as done in [30, 39]. This form directly generates the Jacobians needed to efficiently solve the response with nonlinear implicit integration schemes [40]. The unconstrained coordinates \mathbf{p}_u always satisfy the appropriate compatibility condition, and are related to the constrained coordinates through the connectivity matrix \mathbf{L} . The compatibility condition and hence the connectivity matrix required to assemble the subcomponent models depends on the type of characteristic constraint modes (system-level or local) used to generate the reduced modal equations; the approach for each basis is discussed below.

1. Compatibility with System-level Characteristic Constraint Modes

Compatibility is explicitly enforced for the S-CC modes since they are computed from the linear mass and stiffness matrices associated with the boundary DOF of the assembled CB models. As a result, it can be shown that the generalized coordinates of each characteristic constraint mode in Eq. (8) must be equal, meaning that

$\mathbf{q}_c^{(A)} = \mathbf{q}_c^{(B)} = \mathbf{q}_c$. The substructure coupling matrix \mathbf{L} relating the constrained coordinates to the unconstrained coordinates is defined as,

$$\begin{Bmatrix} \mathbf{p}^{(A)} \\ \mathbf{p}^{(B)} \end{Bmatrix} = \begin{Bmatrix} \mathbf{q}_{k_A}^{(A)} \\ \mathbf{q}_c^{(A)} \\ \mathbf{q}_{k_B}^{(B)} \\ \mathbf{q}_c^{(B)} \end{Bmatrix} = \begin{bmatrix} \mathbf{I} & \mathbf{0} & \mathbf{0} \\ \mathbf{0} & \mathbf{0} & \mathbf{I} \\ \mathbf{0} & \mathbf{I} & \mathbf{0} \\ \mathbf{0} & \mathbf{0} & \mathbf{I} \end{bmatrix} \begin{Bmatrix} \mathbf{q}_{k_A}^{(A)} \\ \mathbf{q}_{k_B}^{(B)} \\ \mathbf{q}_c \end{Bmatrix} = \mathbf{L}\mathbf{p}_u \quad (18)$$

This approach guarantees compatibility at each physical boundary DOF (i.e. $\mathbf{x}_b^{(A)} = \mathbf{x}_b^{(B)}$).

2. Compatibility with Local Characteristic Constraint Modes

The local characteristic constraint modes do not *a priori* account for compatibility at the interface, and as a result the constraints at the boundary DOF, \mathbf{x}_b , must be weakened (i.e. $\mathbf{x}_b^{(A)} \approx \mathbf{x}_b^{(B)}$ in a least-squares sense). The two subcomponent models (A) and (B) can be assembled by defining the L-CC modal coordinates of (A), $\mathbf{q}_c^{(A)}$, as the independent boundary DOF, and those of (B), $\mathbf{q}_c^{(B)}$, as the dependent DOF, making the compatibility condition,

$$\mathbf{q}_c = \mathbf{q}_c^{(A)} = \left(\Psi_{L-CC}^{(A)} \right)^\dagger \Psi_{L-CC}^{(B)} \mathbf{q}_c^{(B)} \quad (19)$$

where the superscript $()^\dagger$ denotes the pseudo inverse operation. With this condition, the substructure coupling matrix \mathbf{L} is defined to eliminate the redundant DOF, which in this case are the L-CC modal coordinates of subcomponent (B). Similar to Eq. (18), this becomes,

$$\begin{Bmatrix} \mathbf{p}^{(A)} \\ \mathbf{p}^{(B)} \end{Bmatrix} = \begin{Bmatrix} \mathbf{q}_{k_A}^{(A)} \\ \mathbf{q}_c^{(A)} \\ \mathbf{q}_{k_B}^{(B)} \\ \mathbf{q}_c^{(B)} \end{Bmatrix} = \begin{bmatrix} \mathbf{I} & \mathbf{0} & & \mathbf{0} \\ \mathbf{0} & \mathbf{0} & & \mathbf{I} \\ \mathbf{0} & \mathbf{I} & & \mathbf{0} \\ \mathbf{0} & \mathbf{0} & \left(\Psi_{L-CC}^{(A)} \right)^\dagger \Psi_{L-CC}^{(B)} & \mathbf{I} \end{bmatrix} \begin{Bmatrix} \mathbf{q}_{k_A}^{(A)} \\ \mathbf{q}_{k_B}^{(B)} \\ \mathbf{q}_c \end{Bmatrix} = \mathbf{L}\mathbf{p}_u \quad (20)$$

Due to the truncation of local characteristic constraint modes, not every physical DOF at the boundary can be enforced with compatibility, resulting in a weaker constraint at the interface.

The assembled equations of motion in Eq. (17) are written in terms of the connectivity matrix \mathbf{L} , and each of the subcomponent CC-NLROMs identified in the previous subsection. The free or forced response to a given initial condition or time varying external force can be integrated using the reduced order model in Eq. (17) at a significantly lower cost than directly integrating a full order FEA model of the assembly. The modal substructuring methodology is demonstrated in the next section by computing the nonlinear normal modes of the ROM in Eq. (17) with various combinations of component modes included in basis. This comparison is conceptually similar to a mesh convergence study for linear systems, and has been shown to effectively gauge the accuracy of a nonlinear ROM [28, 30, 37, 38].

III. Numerical Results: Coupling Elastic Plates with Continuous Interface

The nonlinear modal substructuring approach was applied to the assembly of two geometrically nonlinear, flat plates coupled to one another along a continuous interface. Each plate had simple supports at all nodes around the edges, and was modeled in Abaqus®. A schematic of these FEA models is shown in Fig. 1, where the two substructures were coupled at all x, y, and z rotational DOF along a shared edge. The 9 inch by 9 inch (229 mm by 229 mm) plate was modeled with 1,296 S4R shell elements (a 36×36 grid), while the 9 inch by 6 inch (229 mm by 152 mm) plate had a total of 864 S4R shell elements. Each plate had a uniform thickness of 0.031 inches (0.787 mm); thin-walled structures such as these can experience large deformations even while the materials remain within their elastic range. The material properties were those of structural steel having a Young's modulus of 29,700 ksi (204.8 GPa), shear modulus of 11,600 ksi (80 GPa), and mass density of $7.36 \cdot 10^{-4} \text{ lb-s}^2/\text{in}^4$ ($7,870 \text{ kg/m}^3$). A total of 37 nodes were along the connection points, meaning there were 111 DOF at the interface.

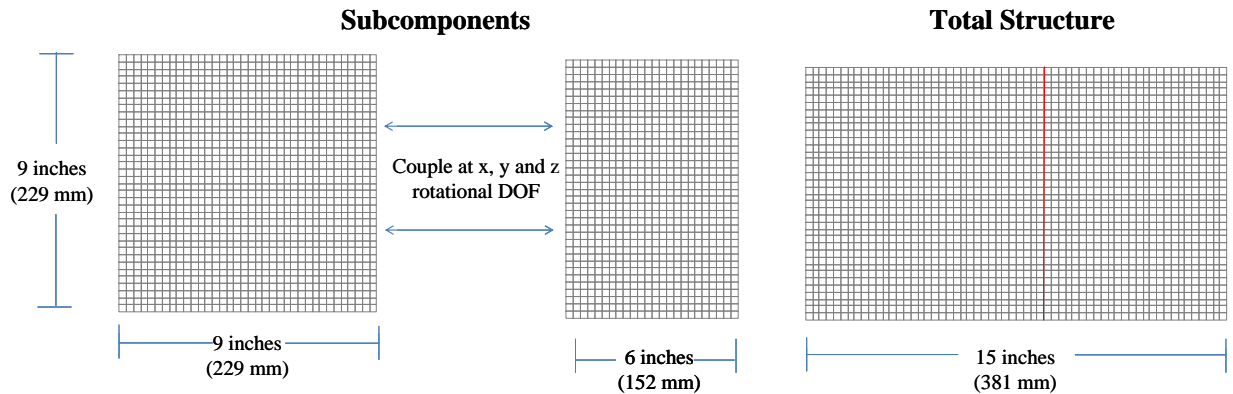


Figure 1. Schematic of coupling two geometrically nonlinear plates with simple supports at all edges. The FEA model of the *total structure* has simple supports at all edges and DOF along the red line where two plates join.

A. Linear Substructuring Results

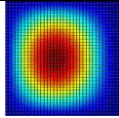
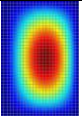
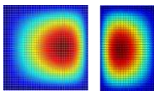
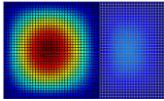
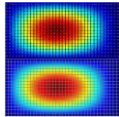
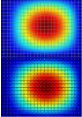
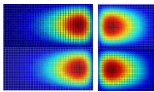
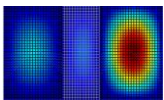
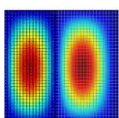
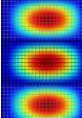
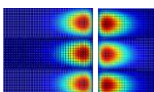
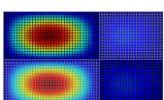
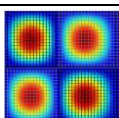
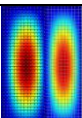
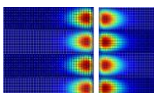
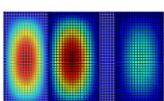
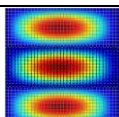
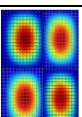
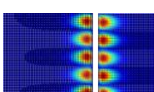
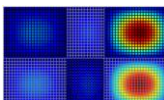
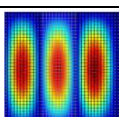
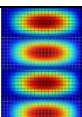
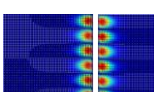
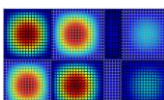
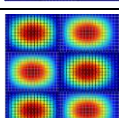
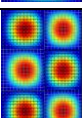
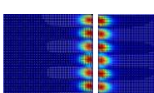
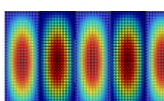
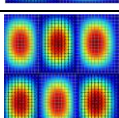
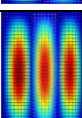
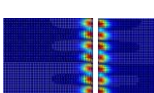
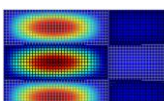
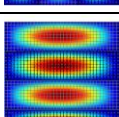
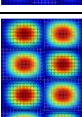
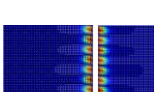
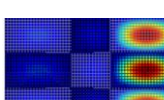
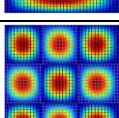
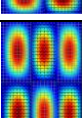
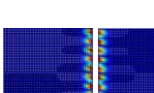
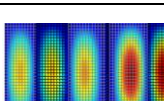
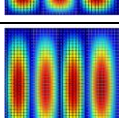
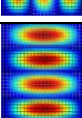
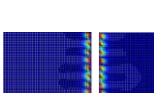
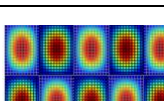
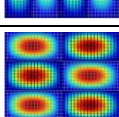
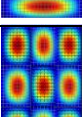
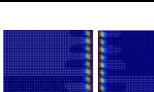
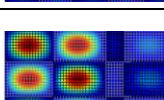
The linear FEA models of the plates were first used to evaluate the *linear* substructuring problem, which provides insight into the basis selection for the nonlinear substructuring problem. The first 12 system-level and local characteristic constraint modes were computed for each plate and compared to one another in Table 1. The analysis shows that each L-CC mode has a MAC value of 1.00 when compared to the S-CC mode (note that the shapes for the S-CC modes are shown later in Table 2), suggesting that the system-level and local approach produces the same shape. The only difference is the associated frequencies from the secondary modal analysis. Recall that the S-CC modes have the same frequencies since they are computed from the mass and stiffness of the assembled CB ROMs. The first three L-CC modes for the two plates have different frequencies, but agree with one another starting with the 4th mode.

Table 1. Comparison of system-level and local characteristic constraint modes.

Characteristic Constraint Mode Number	System-level CC modes	Local CC modes for 9-inch plate		Local CC modes for 6-inch plate	
	Frequency (Hz)	Frequency (Hz)	MAC	Frequency (Hz)	MAC
1	140.2	120.3	1.00	171.1	1.00
2	420.9	412.5	1.00	429.4	1.00
3	930.7	928.9	1.00	930.7	1.00
4	1661	1658	1.00	1658	1.00
5	2610	2606	1.00	2606	1.00
6	3785	3778	1.00	3778	1.00
7	5196	5185	1.00	5185	1.00
8	6853	6837	1.00	6837	1.00
9	8769	8747	1.00	8747	1.00
10	10960	10930	1.00	10930	1.00
11	13440	13400	1.00	13400	1.00
12	16240	16190	1.00	16190	1.00

Since the S-CC and L-CC mode shapes are practically the same for this problem, the linear substructuring analysis is demonstrated with the system-level characteristic constraint modes. Table 2 gives the natural frequencies and mode shapes of the fixed-interface and S-CC modes for each subcomponent model. The exact modes of the full FEA model of the assembly are shown in the far right column to provide a reference solution against which to compare the substructuring results that will be presented later.

Table 2. Linear subcomponent modes used with the fixed-interface and S-CC mode reduction.

Mode Number	Fixed-interface modes: 9"x9" plate	Fixed-interface modes: 9"x6" plate	System-level characteristic constraint modes	Truth modes of total structure
1	 87.1 Hz	 156.8 Hz	 140.2 Hz	 78.4 Hz
2	 190.6 Hz	 254.4 Hz	 420.9 Hz	 135.1 Hz
3	 216.6 Hz	 430.1 Hz	 930.7 Hz	 185.7 Hz
4	 317.7 Hz	 449.5 Hz	 1660 Hz	 203.0 Hz
5	 371.4 Hz	 547.0 Hz	 2610 Hz	 239.5 Hz
6	 420.3 Hz	 685.2 Hz	 3785 Hz	 306.4 Hz
7	 494.6 Hz	 717.4 Hz	 5196 Hz	 365.7 Hz
8	 521.5 Hz	 915.3 Hz	 6853 Hz	 368.2 Hz
9	 630.0 Hz	 965.6 Hz	 8769 Hz	 419.7 Hz
10	 696.1 Hz	 1014 Hz	 10.96 kHz	 434.1 Hz
11	 700.6 Hz	 1021 Hz	 13.44 kHz	 474.4 Hz
12	 749.8 Hz	 1183 Hz	 16.24 kHz	 485.5 Hz

For this example, the frequency range of interest was 0-500 Hz, so the first 12 modes of the total structure in Table 2 were taken as target modes. A typical rule of thumb for linear substructuring is to include subcomponent modes up to 1.5 to 2.0 times this range. Even though the system-level characteristic constraint modes have associated eigenfrequencies from the secondary modal analysis in Eq. (7), this rule of thumb is not well established for these modes. When deciding which S-CC modes to retain in the basis, it was determined that these should be selected such that the accuracy of the CB substructuring approach was preserved. This was done by computing the maximum percent frequency errors between the modes predicted by the assembled CB ROMs, and those from the assembly of truncated S-CC ROMs. This is demonstrated on the linear plates with subcomponent fixed-interface modes up to 750 Hz, 1,000 Hz and 1,500 Hz, or 1.5, 2.0 and 3.0 times the frequency band of interest, respectively. The maximum of the percent frequency error between all the modes predicted by the assembled S-CC ROMs and the assembled CB ROMs is shown in Fig. 2 as S-CC modes were added to the basis. As the number of S-CC modes increases the error precipitously falls down below 0.01%, hence for each case the number of S-CC modes included was chosen such that the maximum percent error in the linear frequencies fell below 0.01 %. Returning to Table 2, one can see that the maximum frequency of the S-CC modes that were included is beyond the frequency range of interest in each case.

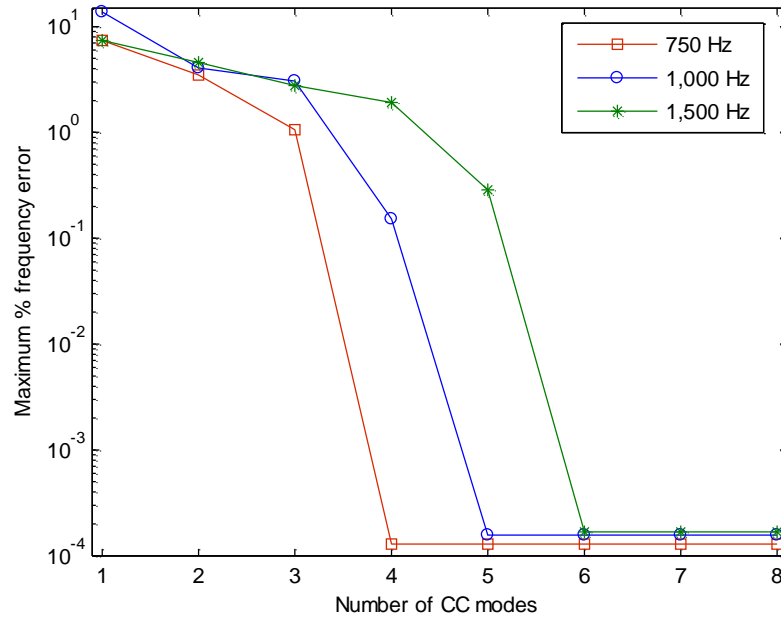


Figure 2. Maximum percent error of the assembly modes predicted by the CB ROMs and the S-CC ROMs as the number of S-CC modes were increased in the basis. The lines represent the number of fixed-interface modes included in each ROM: up to (red squares) 750 Hz, (blue circles) 1,000 Hz and (green asterisks) 1,500 Hz.

Hence, four, five and six S-CC modes were included in the ROM basis for the cases where the fixed-interface modes were included up to 750 Hz, 1,000 Hz, and 1,500 Hz, respectively. The total number of DOF in each of the assembled reduced order models was then 23, 30, and 44 DOF. Even after truncating the S-CC modes in this manner, the resulting model still provides the same predictive accuracy as the full assembled CB ROMs, which have 111 constraint modes. The percent frequency errors in Table 3 compare the predicted modes with those of the full FEA model of the total structure, providing insight into the accuracy of these assembled S-CC ROMs (and ultimately the CB substructuring approach). The lowest order ROM predicted the assembly modes up to 500 Hz very well including linear modes up to only 1.5 times the frequency band of interest; the largest frequency error was 0.39 % in the 11th mode. Additional modes in the basis lowered the frequency error further, as expected. The last column of Table 3 compares the linear substructuring results with a ROM created with 6 local characteristic constraint modes for each plate, and fixed-interface modes up to 1,500 Hz. This modal basis performs quite well when predicting the natural frequencies of the assembly modes, comparable to the S-CC modal basis.

Table 3. Percent frequency error of the first 12 assembly modes predicted by the assembled S-CC/L-CC ROMs and the full FEA model of the total structure.

Total Structure Mode Number	% Error with 4 S-CC modes and up to 750 Hz fixed-interface modes	% Error with 5 S-CC modes and up to 1,000 Hz fixed-interface modes	% Error with 6 S-CC modes and up to 1,500 Hz fixed-interface modes	% Error with 6 L-CC modes and up to 1,500 Hz fixed-interface modes
1	$4.4 \cdot 10^{-4}$	$1.7 \cdot 10^{-4}$	$6.7 \cdot 10^{-5}$	$-6.5 \cdot 10^{-3}$
2	$7.2 \cdot 10^{-3}$	$4.8 \cdot 10^{-3}$	$4.0 \cdot 10^{-3}$	$-2.5 \cdot 10^{-3}$
3	$1.2 \cdot 10^{-3}$	$-1.8 \cdot 10^{-4}$	$-1.3 \cdot 10^{-3}$	$-5.4 \cdot 10^{-3}$
4	$7.4 \cdot 10^{-3}$	$4.0 \cdot 10^{-3}$	$2.8 \cdot 10^{-3}$	$1.1 \cdot 10^{-3}$
5	$1.4 \cdot 10^{-2}$	$6.8 \cdot 10^{-3}$	$8.5 \cdot 10^{-4}$	$-7.0 \cdot 10^{-3}$
6	$1.9 \cdot 10^{-2}$	$9.8 \cdot 10^{-3}$	$2.3 \cdot 10^{-3}$	$-1.1 \cdot 10^{-3}$
7	0.16	$6.2 \cdot 10^{-2}$	$2.7 \cdot 10^{-2}$	$2.2 \cdot 10^{-2}$
8	$5.7 \cdot 10^{-3}$	$3.8 \cdot 10^{-3}$	$1.7 \cdot 10^{-3}$	$-4.4 \cdot 10^{-4}$
9	$2.0 \cdot 10^{-2}$	$1.1 \cdot 10^{-2}$	$2.1 \cdot 10^{-3}$	$-3.3 \cdot 10^{-3}$
10	$1.5 \cdot 10^{-2}$	$5.7 \cdot 10^{-3}$	$2.4 \cdot 10^{-3}$	$2.2 \cdot 10^{-3}$
11	0.39	0.18	$3.3 \cdot 10^{-2}$	$2.3 \cdot 10^{-2}$
12	$2.4 \cdot 10^{-2}$	$1.3 \cdot 10^{-2}$	$3.1 \cdot 10^{-3}$	$-1.6 \cdot 10^{-4}$

For a linear system, the S-CC ROMs with modes up to 750 Hz and 4 S-CC modes would be sufficient for response prediction. In the next subsection, all of these bases are used to compare the nonlinear substructuring approach since additional modes might be necessary to capture the dynamics of the nonlinear assembly. The system-level characteristic constraint modes are used to generate the nonlinear reduced order models, which will be referred as CC-NLROMs, of the geometrically nonlinear plates in Fig. 1. The accuracy of the nonlinear substructuring approach is evaluated using nonlinear normal modes to capture a range of frequency and energy of operation.

B. Nonlinear Substructuring Results

The CC-NLROMs of the two plate models were generated with the same set of fixed-interface and system-level characteristic constraint modes used in the linear analysis (fixed-interface modes up to 750 Hz, 1,000 Hz and 1,500 Hz with 4, 5 and 6 S-CC modes, respectively). When generating the force permutations for the static loads in Eq. (15), the force amplitudes \hat{f} for each mode are typically chosen such that when a single-mode force (e.g. $\mathbf{F}_r = \mathbf{K}\mathbf{T}_{S-CC,r}\hat{f}_r$) is applied to the linear FEA model, the maximum displacement is on the order of one thickness. For the CC-NLROMs generated here, each mode in the \mathbf{T}_{S-CC} basis was scaled to force the linear system to a maximum displacement of 0.25 times the thickness, or $7.75 \cdot 10^{-3}$ inches (0.197 mm). More details on the scaling can be found in [8, 28, 30]. Once the coefficients in Eq. (14) were identified, the CC-NLROMs were coupled and the

equations of motion in Eq. (17**Error! Reference source not found.**) were used to compute the nonlinear normal modes [36] using the continuation algorithm in [41]. The first three NNMs from the assembled CC-NLRROMs are compared with the NNMs of the full FEA model of the total structure in Fig. 3. The full order model NNMs were computed using the applied modal force (AMF) algorithm in [42], which non-intrusively computes the NNMs directly from a finite element model within its native code. These curves were quite expensive to compute since the model had >10,000 DOF. These provide a reference solution to compare the accuracy of the assembled CC-NLRROMs, analogous to the comparison of linear normal modes in the previous subsection.

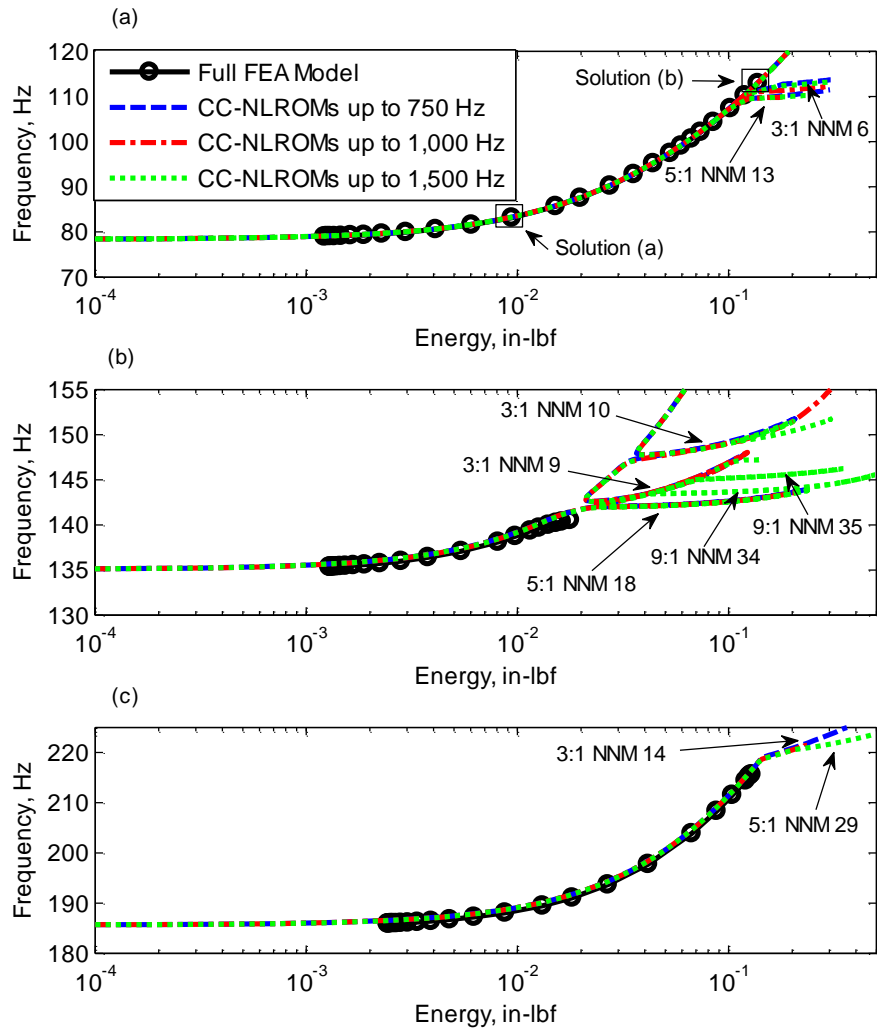


Figure 3. Frequency-energy plots of (a) NNM 1, (b) NNM 2 and (c) NNM 3 for the assembly of two plates in Fig. 1. Each curve was computed from the (black dotted) full order model of the total structure, assembled CC-NLROMs with fixed-interface modes up to (blue dashed) 750 Hz, (red dash-dotted) 1,000 Hz, and (green dotted) 1,500 Hz.

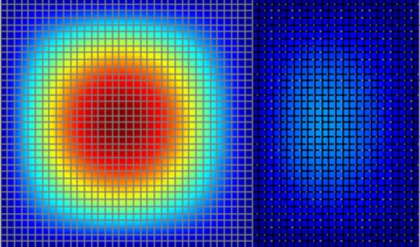
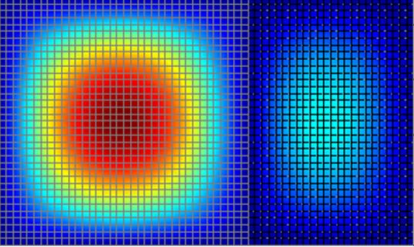
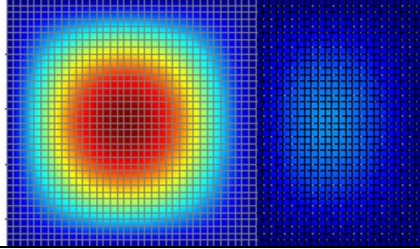
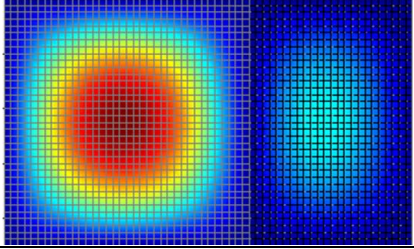
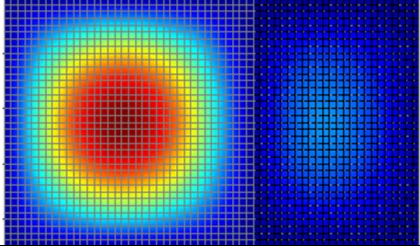
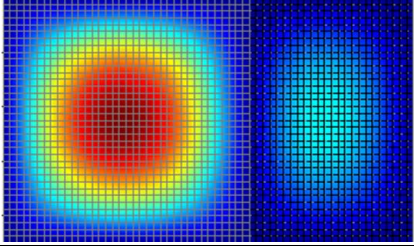
The first three NNMs of the plate assembly exhibit hardening nonlinear behavior as indicated by the increase in frequency with an increase in response energy; this is due to the membrane-bending coupling induced by large bending deformations. Each NNM branch in Fig. 3 started at a linear mode solution at low energy (or response amplitude), but increasing displacement amplitudes exercised the nonlinear restoring force in the equations of motion, changing the dynamic response. There are two notable features of the NNM branches in Fig. 3, namely the backbone, which occurs at the lowest possible energy for a given frequency, and the tongues, which emanate from the backbone. Each tongue corresponds to a modal interaction with other NNMs that oscillate at a strict integer ratio

of frequencies (see [36, 43] for further discussion of these solutions). AMF was run in a manner that caused all of its solutions (black circles) to remain along the main backbone; further computations would be needed to capture these modal interactions.

The main backbones predicted by all of the assembled CC-NLROMs agree very well with those of the full order model, suggesting that even the lowest order model (with fixed-interface modes up to 750 Hz and 4 CC modes) could be used for accurate response prediction. Adding fixed-interface and S-CC modes to the basis did slightly affect the modal interactions predicted by the ROMs. For example, in Fig. 3c the modal interaction near 220 Hz started as a 3:1 interaction with NNM 14 (i.e. mode 14 oscillates at a frequency 3 times the fundamental frequency of ~220 Hz). The 750 Hz assembly of CC-NLROMs (blue dashed) continued along this tongue towards higher energies, whereas the 1,500 Hz assembly (green dotted) continued along a new tongue corresponding to a 5:1 interaction with NNM 29. Since the 750 Hz model only had 23 DOF it would not be able to compute NNM 29, meaning that higher order ROMs were needed to capture these responses. Similar observations are made in Fig. 3b with the tongues emanating from the 3:1 interaction with NNM 9. The 1,500 Hz assembly of CC-NLROMs captured the 9:1 interactions with NNMs 34 and 35, both of which were not captured with the lower order models. An infinite number of these interactions can occur along the backbone of the NNM, and it is hard to determine the effect of these solutions on the accuracy of the ROMs.

The higher order NNMs 4 through 10 computed with the 750 Hz and 1,500 Hz models were in agreement along the backbones, however NNM 11 was the first to show a slight disagreement (these results are not shown for brevity). This nonlinear convergence study helps identify when a sufficient number of modes have been included in the basis for the frequency bandwidth of interest. To further compare each model, the maximum out-of-plane displacements (i.e. when the velocity is zero) are shown in Table 4 for the solutions marked (a) and (b) in Fig. 3a using the full order model, and the two assemblies of CC-NLROMs with fixed-interface modes up to 750 Hz and 1,500 Hz. The deformations predicted by the ROMs agree very well with the full order model; each ROM had a maximum error in out-of-plane displacement of 0.8% for solution (a), and 0.4% for solution (b). This match was expected from the agreement with the frequency-energy plots shown earlier. It is interesting to note that the deformations change as the energy increases along the backbone. More vibration energy was in the smaller 9 inch by 6 inch (229 mm by 152 mm) plate at solution (b) as compared with solution (a), which was taken near the linear regime.

Table 4. Table comparing the out-of-plane maximum deformation shapes of solutions (a) and (b) marked along NNM 1 in Fig. 3.

Model	Solution (a) at 83.2 Hz	Solution (b) at 112.9 Hz
Full Order Model		
CC-NLRoms with modes up to 750 Hz		
CC-NLRoms with modes up to 1,500 Hz		

The NNMs computed from the undamped equations of motion in Eq. (17) **Error! Reference source not found.** have an intimate connection to the forced steady state response of the damped system, as these undamped NNMs form the backbone to the forced response curves [36, 43-46]. Resonance of the damped response occurs in the neighborhood of the NNM when the damping forces exactly cancel out the harmonic forcing function. Therefore, by accurately capturing the NNMs, the damped forced response near resonance, which is when the structure is at its greatest risk of failure, will also be accurate. Hence, the results presented above suggest that either of the CC-NLRoms would accurately capture the forced response of the panel near resonance.

During the course of this research, it was questioned whether it was truly important to capture the nonlinear stiffness of the characteristic constraint modes and their nonlinear couplings to the other modes. It was hypothesized that these terms might be negligible, in which case one could simply create a ROM from the fixed-interface structure, augment it with *linear* CC modes, and compute the response of the assembly. To test this hypothesis, a separate modeling strategy was explored during this research where each nonlinear subcomponent ROM was estimated by fixing all of the boundary DOF in the FEA model in Eq. (11), computing the nonlinear modal model

from it using only the fixed-interface modes, and appending the linear CC modes without any nonlinear coupling in the modal equations of motion. These subcomponent models are referred to here as fixed-interface NLROMs (FI-NLROMs), and were assembled in the same way as the CC-NLROMs. This approach was motivated by the potential computational savings obtained by only requiring static force permutations in Eq. (15) in the shapes of the fixed-interface modes, and not the static constraint modes. For example, for the ROMs of the 9 by 9 inch (229 mm by 229 mm) plate with fixed-interface modes up to 1,500 Hz, this would require only 15,226 load cases instead of 30,914 for the CC-NLROM. Unfortunately, this approach was found to produce an inaccurate estimate of the first NNM, as shown in Fig. 4.

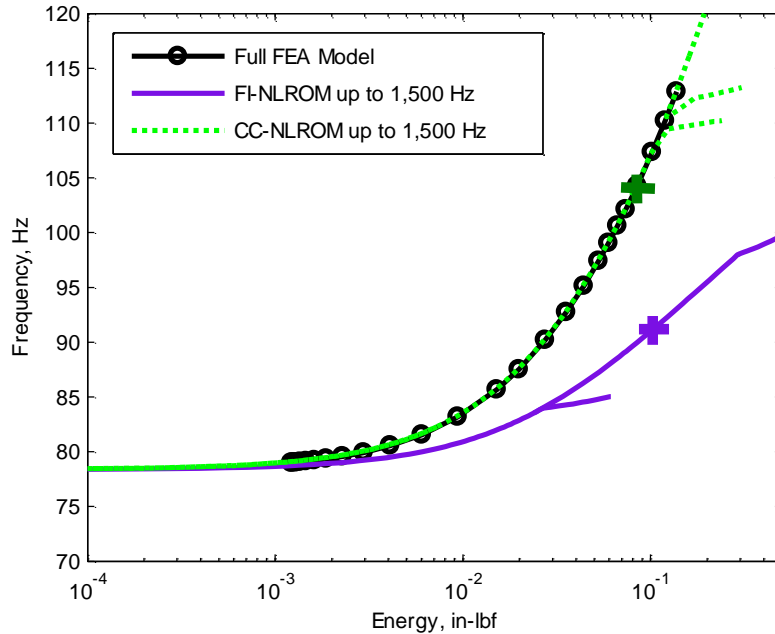


Figure 4. Frequency-energy plots of NNM 1 for the assembly of two plates. Each curve was computed from (black dotted) full order model of the total structure, (green dotted) assembled CC-NLROMs and (purple solid) assembled FI-NLROMs with fixed-interface modes up to 1,500 Hz.

The NNM predicted by the assembled FI-NLROMs with fixed-interface modes up to 1,500 Hz (and 6 linear CC modes) clearly disagrees with that predicted by the assembled CC-NLROMs with the same basis and the full FEA model. In order to quantify the importance of these results, the energy balance technique in [43, 47, 48] was used to compute the force amplitude required to excite resonance of the damped system with a single-point harmonic forcing function. In this calculation, each mode of the FI-NLROMs and CC-NLROMs was assumed to have 0.1% modal damping, which is near the damping level observed experimentally for similar structures [8]. A point force

was applied at the midpoint of the 9 inch by 9 inch (229 mm by 229 mm) plate in the out-of-plane direction. This analysis predicted that a point force with an amplitude of $9.6 \cdot 10^{-3}$ lbf ($4.3 \cdot 10^{-2}$ N) would excite resonance of the assembled FI-NLROMs at 90 Hz, resulting in a peak displacement of 0.0328 inches (0.833 mm). The calculations with the more accurate ROM predicted that this force amplitude would actually produce resonance at a significantly higher frequency (104.3 Hz) with a smaller peak displacement of 0.0295 inches (0.749 mm). The corresponding locations are marked with a (+) in Fig. 4. The accuracy of the modeling strategy and its resulting NNMs have a strong connection to the accuracy of the various forced response predictions.

The AMF algorithm took on the order of 2 to 3 days to compute each NNM of the 12,861 DOF full order model of the assembly using a desktop computer with an Intel® Core i7 CPU and 8 GB of RAM, so only a few "truth" solutions were available for comparison throughout this section. Each NNM from the CC-NLROM substructuring approach took anywhere from 15-30 minutes to compute, depending on the parameters used in the stepsize controller and the size of the ROM. The upfront cost to run the static analyses for each CC-NLROM is summarized in Table 5, along with the cost estimate if all 111 static constraint modes were used in the basis without any interface reduction (note that this would be the CB-NLROM approach in [30, 32]). For example, creating the CC-NLROMs with fixed-interface modes up to 1,500 Hz and 6 CC modes would require a total of 42,436 static load cases, taking 46 hours on the desktop computer mentioned earlier, and the equivalent CB-NLROMs would require 5,808,336 static loads and 248 days of CPU time. The interface reduction reduced the number of static loads required by ICE approach to identify each subcomponent model, making the modal substructuring approach feasible. For reference, creating an NLROM of the full plate assembly with linear modes up to 500 Hz and 1,500 Hz (a total of 12 and 41 modal DOF, respectively) would require 2,048 static loads (4 hours) and 88,642 static loads (173 hours), respectively. In practice, this model would likely need more than modes up to 500 Hz to accurately capture all the NNMs in the 0-500 Hz frequency range, however this serves as the lower bound to the cost estimate.

Table 5. Computational cost associated with the identification of nonlinear subcomponent models using ICE.

Model	Fixed-interface modes up to 750 Hz		Fixed-interface modes up to 1,000 Hz		Fixed-interface modes up to 1,500 Hz	
	CB-NLROM	CC-NLROM	CB-NLROM	CC-NLROM	CB-NLROM	CC-NLROM
9 inch by 9 inch plate	·123 DOF ·2,451,226 loads ·122 days	·16 DOF ·4,992 loads ·6 hours	·127 DOF ·2,699,258 loads ·134 days	·21 DOF ·11,522 loads ·14 hours	·134 DOF ·3,172,584 loads ·158 days	·29 DOF ·30,914 loads ·37 hours
9 inch by 6 inch plate	·118 DOF ·2,163,176 loads	·11 DOF ·1,562 loads ·1 hour	·120 DOF ·2,275,520 loads	·14 DOF ·3,304 loads ·3 hours	·126 DOF ·2,635,752 loads	·21 DOF ·11,522 loads ·9 hours

	·74 days		·78 days		·90 days	
--	----------	--	----------	--	----------	--

IV. Conclusions

This paper presented a nonlinear modal substructuring approach for geometrically nonlinear structures by creating nonlinear subcomponent models with the Implicit Condensation and Expansion method [8, 9] using fixed-interface modes and system-level characteristic constraint modes [12] as a basis. These low order models are assembled to provide a reduced order model that accounts for nonlinear effects. The interface reduction could be carried out with either system-level or local characteristic constraint modes to drastically reduce the number of DOF describing the interface, hence lowering the upfront computational cost associated with the identification of the nonlinear stiffness coefficients in the subcomponent models. The synthesized CC-NLROMs are orders of magnitude smaller compared to the full order finite element model yet maintain acceptable accuracy. A substructuring approach has the advantage of dealing with several small, simpler subcomponent models compared to one large complicated model. Often during the development and analysis of structural components, most design changes occur at a subcomponent level, therefore a modal substructuring approach makes it easier to update one subcomponent model rather than the entire model of the assembly.

The substructuring approach with CC-NLROMs was demonstrated by coupling two thin plates with geometric nonlinearity. The NNMs were computed from the assembled CC-NLROMs equations generated with an increasing number of fixed-interface and system-level characteristic constraint modes. The results showed excellent agreement along the backbone predicted by each ROM and the full order model. The only difference with the higher order ROMs is the computed modal interactions along the NNM branch, which account for interactions with higher order NNMs. The results show how the maximum deformation shape evolves along the backbone of NNM 1, providing helpful insight into the evolution of the stress fields experienced by the system at various resonant conditions. The NNMs serve as a signature of the equations that quickly identify whether or not a model captures some important solutions of the full order model; if the reference NNMs solutions were not available, the convergence of the CC-NLROMs would suggest the models have a sufficient basis to capture the NNMs, making this a powerful comparison metric. Due to the intimate connection between the NNMs and the forced, damped response, a ROM that can accurately predict the NNMs will likely predict the response to other load scenarios [28, 36, 38, 44-48].

Acknowledgments

The authors gratefully acknowledge the support of the Air Force Office of Scientific Research under grant award number FA9550-11-1-0035, administered by the Multi-Scale Structural Mechanics and Prognosis program managed by David Stargel. RJK would also like to acknowledge funding from the National Physical Science Consortium (NPSC) Fellowship for this research.

References

1. Crisfield, M. A., *Nonlinear finite element analysis of solids and structures. Volume 1: Essentials*. Wiley, New York, 1991.
2. Crisfield, M. A. *Nonlinear finite element analysis of solids and structures. Volume 2: Advanced Topics*. Wiley, New York, 1991.
3. Muravyov, A. A., and Rizzi, S. A., "Determination of nonlinear stiffness with application to random vibration of geometrically nonlinear structures," *Computers & Structures*, Vol. 81, No. 15, 2003, pp. 1513-1523.
doi: 10.1016/s0045-7949(03)00145-7
4. Przekop, A., Guo, X., and Rizzi, S. A., "Alternative modal basis selection procedures for reduced-order nonlinear random response simulation," *Journal of Sound and Vibration*, Vol. 331, No. 17, 2012, pp. 4005-4024.
doi: [10.1016/j.jsv.2012.03.034](https://doi.org/10.1016/j.jsv.2012.03.034)
5. Rizzi, S. A., and Przekop, A., "Estimation of Sonic Fatigue by Reduced-Order Finite Element Based Analyses," *Proceedings of the Ninth International Conference on Recent Advances in Structural Dynamics* [CD-ROM], The Inst. of Sound and Vibration, Southampton, England, U.K., 2006.
6. Rizzi, S. A., and Przekop, A., "System identification-guided basis selection for reduced-order nonlinear response analysis," *Journal of Sound and Vibration*, Vol. 315, No. 3, 2008, pp. 467-485.
doi: [10.1016/j.jsv.2007.12.031](https://doi.org/10.1016/j.jsv.2007.12.031)
7. Rizzi, S. A., and Przekop, A. "The Effect of Basis Selection on Static and Random Acoustic Response Prediction Using a Nonlinear Modal Simulation," NASA Rept. TP-2005-213943, Dec. 2005.
8. Gordon, R. W., and Hollkamp, J. J., "Reduced-Order Models for Acoustic Response Prediction," U.S. Air Force Research Lab. Report RB-WP-TR-2011-3040, Jul. 2011.
9. Hollkamp, J. J., and Gordon, R. W., "Reduced-order models for nonlinear response prediction: Implicit condensation and expansion," *Journal of Sound and Vibration*, Vol. 318, No. 4, 2008, pp. 1139-1153.
doi: 10.1016/j.jsv.2008.04.035
10. Hollkamp, J. J., Gordon, R. W., and Spottswood, S. M., "Nonlinear modal models for sonic fatigue response prediction: a comparison of methods," *Journal of Sound and Vibration*, Vol. 284, No. 3-5, 2005, pp. 1145-1163.
doi: 10.1016/j.jsv.2004.08.036
11. O'Hara, P. J., and Hollkamp, J. J., "Modeling vibratory damage with reduced-order models and the generalized finite element method," *Journal of Sound and Vibration*, Vol. 333, No. 24, 2014, pp. 6637-6650.

- doi: [10.1016/j.jsv.2014.07.023](https://doi.org/10.1016/j.jsv.2014.07.023)
12. Castanier, M. P., Tan, Y., and Pierre, C., "Characteristic Constraint Modes for Component Mode Synthesis," *AIAA Journal*, Vol. 39, No. 6, 2001, pp. 1182-1187.
doi: [10.2514/2.1433](https://doi.org/10.2514/2.1433)
 13. Hurty, W. C., "Dynamic analysis of structural systems using component modes," *AIAA Journal*, Vol. 3, No. 4, 1965, pp. 678-685.
doi: [10.2514/3.2947](https://doi.org/10.2514/3.2947)
 14. Craig, R. R. J., and Bampton, M. C. C., "Coupling of Substructures for Dynamic Analysis," *AIAA Journal*, Vol. 6, No. 7, 1968, pp. 1313-1319.
doi: [10.2514/3.4741](https://doi.org/10.2514/3.4741)
 15. R. Craig, J. R., and Chang, C.-J., "On the use of attachment modes in substructure coupling for dynamic analysis," *18th Structural Dynamics and Materials Conference*. AIAA Paper 77-405, 1977.
 16. Rubin, S., "Improved Component-Mode Representation for Structural Dynamic Analysis," *AIAA Journal*, Vol. 13, No. 8, 1975, pp. 995-1006.
doi: [10.2514/3.60497](https://doi.org/10.2514/3.60497)
 17. Hintz, R. M., "Analytical Methods in Component Modal Synthesis," *AIAA Journal*, Vol. 13, No. 8, 1975, pp. 1007-1016.
doi: [10.2514/3.60498](https://doi.org/10.2514/3.60498)
 18. MacNeal, R. H., "A hybrid method of component mode synthesis," *Computers & Structures*, Vol. 1, No. 4, 1971, pp. 581-601.
doi: [10.1016/0045-7949\(71\)90031-9](https://doi.org/10.1016/0045-7949(71)90031-9)
 19. Blelloch, P., and Vold, H. "Orthogonality and large models - what's the problem?," *Proceedings of the 23rd International Modal Analysis Conference (IMAC XXIII)*, Society of Experimental Mechanics, Orlando, FL, 2005.
 20. Hong, S.-K., Epureanu, B. I., and Castanier, M. P., "Next-generation parametric reduced-order models," *Mechanical Systems and Signal Processing*, Vol. 37, No. 1-2, 2013, pp. 403-421.
doi: [10.1016/j.ymsp.2012.12.012](https://doi.org/10.1016/j.ymsp.2012.12.012)
 21. Tran, D. M., "Component mode synthesis methods using interface modes. Application to structures with cyclic symmetry," *Computers & Structures*, Vol. 79, No. 2, 2001, pp. 209-222.
doi: [10.1016/S0045-7949\(00\)00121-8](https://doi.org/10.1016/S0045-7949(00)00121-8)
 22. Witteveen, W., and Irschik, H., "Efficient Mode Based Computational Approach for Jointed Structures: Joint Interface Modes," *AIAA Journal*, Vol. 47, No. 1, 2009, pp. 252-263.
doi: [10.2514/1.38436](https://doi.org/10.2514/1.38436)
 23. Donders, S., Pluymers, B., Ragnarsson, P., Hadjit, R., and Desmet, W., "The wave-based substructuring approach for the efficient description of interface dynamics in substructuring," *Journal of Sound and Vibration*, Vol. 329, No. 8, 2010, pp. 1062-1080.
doi: [10.1016/j.jsv.2009.10.022](https://doi.org/10.1016/j.jsv.2009.10.022)
 24. Mignolet, M. P., Przekop, A., Rizzi, S. A., and Spottswood, S. M., "A review of indirect/non-intrusive reduced order modeling of nonlinear geometric structures," *Journal of Sound and Vibration*, Vol. 332, No. 10, 2013, pp. 2437-2460.
doi: [10.1016/j.jsv.2012.10.017](https://doi.org/10.1016/j.jsv.2012.10.017)

25. McEwan, M. I., Wright, J. R., Cooper, J. E., and Leung, A. Y. T., "A Combined Modal/Finite Element Analysis Technique for the Dynamic Response of a Non-linear Beam to Harmonic Excitation," *Journal of Sound and Vibration*, Vol. 243, No. 4, 2001, pp. 601-624.
doi: 10.1006/jsvi.2000.3434
26. Perez, R., Wang, X. Q., and Mignolet, M. P., "Nonintrusive Structural Dynamic Reduced Order Modeling for Large Deformations: Enhancements for Complex Structures," *Journal of Computational and Nonlinear Dynamics*, Vol. 9, No. 3, 2014, pp. 031008-031008.
doi: 10.1115/1.4026155
27. Kim, K., Radu, A. G., Wang, X. Q., and Mignolet, M. P., "Nonlinear reduced order modeling of isotropic and functionally graded plates," *International Journal of Non-Linear Mechanics*, Vol. 49, No. 0, 2013, pp. 100-110.
doi: [10.1016/j.ijnonlinmec.2012.07.008](https://doi.org/10.1016/j.ijnonlinmec.2012.07.008)
28. Kuether, R. J., Deaner, B. J., Hollkamp, J. J., and Allen, M. S., "Evaluation of Geometrically Nonlinear Reduced-Order Models with Nonlinear Normal Modes," *AIAA Journal*, Vol. 53, No. 11, 2015, pp. 3273-3285.
doi: 10.2514/1.J053838
29. Hollkamp, J. J., Gordon, R. W., and Spottswood, S. M. "Nonlinear Sonic Fatigue Response Prediction from Finite Element Modal Models: A Comparison with Experiments," *44th AIAA/ASME/ASCE/AHS/ASC Structures, Structural Dynamics, and Materials Conference*, AIAA Paper 2003-1709, 2003.
30. Kuether, R. J., Allen, M. S., and Hollkamp, J. J., "Modal Substructuring of Geometrically Nonlinear Finite-Element Models," *AIAA Journal*, 2015, pp. 1-12.
doi: 10.2514/1.J054036
31. Perez, R. A., "Multiscale Reduced Order Models for the Geometrically Nonlinear Response of Complex Structures." Ph.D. Dissertation, Arizona State University, Tempe, AZ, 2012.
32. Kuether, R. J., and Allen, M. S., "Craig-Bampton Substructuring for Geometrically Nonlinear Subcomponents," *Proceedings of the 32nd International Modal Analysis Conference (IMAC XXXII)*, Society of Experimental Mechanics, Orlando, FL, 2014.
33. Craig, R. R. J., and Kurdila, A. J., *Fundamentals of Structural Dynamics*, 2nd ed., Wiley, New York, 2006.
34. Ginsberg, J. H., *Mechanical and Structural Vibrations: Theory and Applications*, 1st ed., Wiley, New York, 2001.
35. Kuether, R. J., and Allen, M. S., "Nonlinear Modal Substructuring of Systems with Geometric Nonlinearities," *54th AIAA/ASME/ASCE/AHS/ASC Structures, Structural Dynamics, and Materials Conference*, AIAA Paper 2013-1521, 2013.
36. Kerschen, G., Peeters, M., Golinval, J. C., and Vakakis, A. F., "Nonlinear normal modes. Part I. A useful framework for the structural dynamicist," *Mechanical Systems and Signal Processing*, Vol. 23, No. 1, 2009, pp. 170-94.
doi: 10.1016/j.ymsp.2008.04.002
37. Kuether, R. J., Brake, M. R., and Allen, M. S., "Evaluating Convergence of Reduced Order Models Using Nonlinear Normal Modes," *Proceedings of the 32nd International Modal Analysis Conference (IMAC XXXII)*, Society of Experimental Mechanics, Orlando, FL, 2014.

38. Schoneman, J. D., Allen, M. S., and Kuether, R. J., "Relationships between Nonlinear Normal Modes and Response to Random Inputs," *55th AIAA/ASME/ASCE/AHS/ASC Structures, Structural Dynamics, and Materials Conference*, AIAA Paper 2014-1514, 2014.
39. Nash, M., "Nonlinear Structural Dynamics by Finite Element Modal Synthesis," Ph.D. Dissertation, University of London, Imperial College, London, 1977.
40. Patrick, J. O. H., and Joseph, J. H., "Improved Solution of Nonlinear Reduced-Order Models for Static and Dynamic Response Prediction," *56th AIAA/ASCE/AHS/ASC Structures, Structural Dynamics, and Materials Conference*, AIAA Paper 2015-1168, 2015.
41. Peeters, M., Viguié, R., Sérandour, G., Kerschen, G., and Golinval, J. C., "Nonlinear normal modes, Part II: Toward a practical computation using numerical continuation techniques," *Mechanical Systems and Signal Processing*, Vol. 23, No. 1, 2009, pp. 195-216.
doi: [10.1016/j.ymsp.2008.04.003](https://doi.org/10.1016/j.ymsp.2008.04.003)
42. Kuether, R. J., and Allen, M. S., "A numerical approach to directly compute nonlinear normal modes of geometrically nonlinear finite element models," *Mechanical Systems and Signal Processing*, Vol. 46, No. 1, 2014, pp. 1-15.
doi: [10.1016/j.ymsp.2013.12.010](https://doi.org/10.1016/j.ymsp.2013.12.010)
43. Kuether, R. J., Renson, L., Detroux, T., Grappasonni, C., Kerschen, G., and Allen, M. S., "Nonlinear normal modes, modal interactions and isolated resonance curves," *Journal of Sound and Vibration*, Vol. 351, 2015, pp. 299-310.
doi: [10.1016/j.jsv.2015.04.035](https://doi.org/10.1016/j.jsv.2015.04.035)
44. Cammarano, A., Hill, T. L., Neild, S. A., and Wagg, D. J., "Bifurcations of backbone curves for systems of coupled nonlinear two mass oscillator," *Nonlinear Dynamics*, Vol. 77, No. 1-2, 2014, pp. 311-320.
doi: [10.1007/s11071-014-1295-3](https://doi.org/10.1007/s11071-014-1295-3)
45. Peeters, M., Kerschen, G., and Golinval, J. C., "Dynamic testing of nonlinear vibrating structures using nonlinear normal modes," *Journal of Sound and Vibration*, Vol. 330, No. 3, 2011, pp. 486-509.
doi: [10.1016/j.jsv.2010.08.028](https://doi.org/10.1016/j.jsv.2010.08.028)
46. Vakakis, A. F., Manevitch, L. I., Mikhlin, Y. V., Pilipchuk, V. N., and Zevin, A. A., *Nonlinear Modes and Localization in Nonlinear Systems*. 1st ed., Wiley, New York, 1996.
47. Hill, T. L., Cammarano, A., Neild, S. A., and Wagg, D. J., "An Analytical Method for the Optimisation of Weakly Nonlinear Systems," *Proceedings of the 9th International Conference on Structural Dynamics - EURO DYN 2014*. Porto, Portugal, 2014.
48. Hill, T. L., Cammarano, A., Neild, S. A., and Wagg, D. J., "Interpreting the forced responses of a two-degree-of-freedom nonlinear oscillator using backbone curves," *Journal of Sound and Vibration*, Vol. 349, 2015, pp. 276-288.
doi: [10.1016/j.jsv.2015.03.030](https://doi.org/10.1016/j.jsv.2015.03.030)